Microfluidics and Nanofluidics (2023) 27:82
https://doi.org/10.1007/s10404-023-02686-9

RESEARCH

Flow synthesis of 1-ethyl-3-methylimidazolium ethyl sulfate in a PTFE micro-capillary: an experimental and numerical study

Nirvik Sen[1,2] · K. K. Singh[1,2] · S. Mukhopadhyay[1] · K. T. Shenoy[3]

Received: 24 March 2023 / Accepted: 13 September 2023 / Published online: 23 October 2023

Abstract

In this work, we have reported continuous flow synthesis of 1-ethyl-3-methylimidazolium ethyl sulfate ionic liquid in a PTFE micro-capillary. A Y-shaped microfluidic junction is used to mix the incoming reactants. Effects of independent parameters like velocity, reaction temperature, and micro-capillary diameter on product yield, rate of production, and space–time yield are reported. Yield is seen to increase monotonically as reaction temperature is increased, while it reduces with an increase in diameter of the micro-capillary. A maxima in yield is observed as flow velocity is increased. A space–time yield of 1258.4 g/min.L is obtained at a reaction temperature of 80 ^{0}C using a 300 μm micro-capillary. A two-dimensional computational fluid dynamics (CFD) model of the reacting system has been developed to confirm and explain the observed experimental trends. The simulations were able to qualitatively predict the experimental trends. The simulations also investigated the effect of shapes of different obstacles placed in the flow path.

Keywords Homogeneous catalysis · Ionic liquids · Liquid–liquid reaction · Micro-capillary · Space–time yield

Nomenclature

C_1, C_2	Reactant concentration (1st and 2nd reactants) (mol/ m^3)
C_p	Reaction mixture specific heat capacity (J/kg-K)
d	Micro-capillary diameter (m)
E_a	Activation energy (kJ/mol)
H	Enthalpy/heat of reaction (kJ/mol)
k	Reaction mixture thermal conductivity (W/m–K)
k_0	Frequency factor (m^3/mol-s)
T	Reaction/reactor/tube wall temperature (°C)
$\overline{\mathrm{U}}$	Velocity vector (m/s)
v	Flow velocity (m/s)

Greek letters

ρ	Density (kg/m^3)
μ	Viscosity (kg/m-s)

1 Introduction

Ionic liquids (ILs) are a class of compounds that have an ionic state, a melting point lower than 100 °C, an organic cation and an organic or inorganic anion. Some ILs are liquid at room temperature, and these are called room-temperature ionic liquids (RTILs). One of the main properties of ILs is their ability to dissolve a wide range of materials while having negligible volatility. This makes them attractive as green solvents, as they are non-toxic and have a low environmental impact (Marsh et al. 2004; Earle & Seddon 2000; Zhao 2006). Due to their ionic state, ILs possess high ionic conductivity and offer a large electrochemical window (unlike any molecular solvent) which is often useful when ILs are used in process like electro deposition (Armand et al. 2009; Jayakumar et al. 2011). The physical and chemical properties of ionic liquids (ILs) can be easily adjusted or fine-tuned by carefully selecting the cationic and anionic components (Le Rouzo et al. 2009; Rout et al. 2012). This tailorable nature of ionic liquids (ILs) makes them attractive in various separation processes (Sen et al. 2022, 2017). Because of the above-mentioned advantages, ILs have widely been used in a variety of application like catalysis, organic synthesis, solvent extraction, and electrochemistry (Dai et al. 1999; Giridhar et al. 2008; Meindersma et al. 2006; Ali et al. 2017; Sen et al. 2017; Xu et al. 2019; Hadj-Kali et al. 2020). Traditionally, ionic liquids (ILs) are

✉ Nirvik Sen
nirvik@barc.gov.in

[1] Chemical Engineering Division, Bhabha Atomic Research Centre, Trombay, Mumbai 400085, India

[2] Homi Bhabha National Institute, Mumbai 400094, India

[3] Chemical Engineering Group, Bhabha Atomic Research Centre, Trombay, Mumbai 400085, India

synthesized in semi-batch or batch mode in stirred tanks using a solvent to act as a thermostat to manage the heat of the reaction. Alkylation reactions are highly exothermic, meaning that they release a significant amount of energy during the reaction. If this energy is not released, it can lead to hot spots, which can eventually lead to a thermal runaway. To prevent this, a volatile solvent is used under reflux, which lowers the operating temperature. This solves the problem of temperature management, and it also dilutes the reaction mixture and lowers the reaction temperature, making the reaction itself very slow.

In the last decade, there has been a growing interest in micro-reactors, which are devices that allow reactions to be carried out under flow conditions in channels with a characteristic dimension of less than 1 mm. Micro-reactors have been used to synthesize a wide variety of specialty chemicals and micro/nano-particles (Jankowski et al. 2020; Waterkamp et al. 2009; Ye et al. 2022; Kang et al. 2013; Mou et al. 2022; Zhang et al. 2010). They have been instrumental in converting batch processes to flow processes. They offer various advantages like better selectivity, higher space–time yield, and safer operations to name a few. One of the key features of micro-reactors is their very high surface-to-volume ratio, which leads to very high rates of heat transfer. This makes them ideal for carrying out highly exothermic reactions, such as ionic liquid synthesis, at elevated temperatures and in a solvent-free manner (Waterkamp et al. 2007, 2009; Renken et al. 2007; Sen et al. 2013).

In this work, we report the high-temperature synthesis of 1-ethyl-3-methylimidazolium ethyl sulfate ([EMIM]$EtSO_4$) in a simple micro-capillary without using any solvent. Recently, 1-ethyl-3-methylimidazolium ethyl sulfate ([EMIM]$EtSO_4$) has attracted significant interest from researchers for its potential to remove sulfur compounds from hydrocarbon streams, which is an essential step in hydrocarbon desulphurization (Kulkarni and Afonso 2010; Eβer et al. 2004). This ionic liquid also has the potential to be used in hydrogen production through thermal–chemical cycles. In one of the reactions of the iodine–sulfur cycle (a thermal–chemical process for large-scale hydrogen generation), sulfuric acid is dissociated into water, oxygen, and sulfur dioxide. (Kar et al. 2012; Goswami et al. 2014). Sulfur dioxide needs to be separated from the other products of the Bunsen reaction to be recycled. [EMIM]$EtSO_4$ can be used for this separation. Recently, there has been growing interest in the use of 1-ethyl-3-methylimidazolium ethyl sulfate ([EMIM]EtSO4) as a promising candidate for ionic liquid-based dual/mono-mode propellant for spacecraft propulsion (Li et al. 2021; Berg and Rovey 2013). The use of ionic liquids makes propellants less hazardous than hydrazine and also significantly improves the available density-specific impulse (Whitmore et al. 2013). The controlled delivery of a few tens of microliters of [EMIM]EtSO4-HAN per minute followed by its decomposition over a suitable catalyst (Pt/Al2O3) has been the basis of some designs of chemical micro-thrusters suitable for maneuvering micro-satellites. (Sharma et al. 2022).

The chosen alkylation reaction is exothermic and the specific heat of reaction heat is 102 kJ/mol (Gröbe Böwing and Jess 2007). Accurate temperature control is, thus, essential to prevent thermal runaway and consequent product degradation. Therefore, any reactor used for synthesis or production of this IL must be designed to effectively remove heat. Tubular reactors that operate continuously have been proposed as a way to control this reaction. (Jess et al. 2005; Löb et al. 2006). Millimeter-sized reactors (where reactor diameter is of the order of a few millimeters) were used to increase the specific heat transfer area (i.e., heat transfer area per unit volume of the reactor). This led to improved thermal management.

Renken and coworkers (Renken et al. 2007) reported flow synthesis of [EMIM]$EtSO_4$ in a sequential reactor system. It comprised of a micro-structured reactor followed by 1/8 inch capillary reactor which in turn was followed by another 1/4 inch capillary reactor. The authors mixed the two incoming reactants using a caterpillar-type micro-mixer. The two tubular reactors (1/8 and 1/4 inch) were maintained at different reaction temperatures. A total liquid flow rate of 0.4 L/hr could be processed. The authors reported a reduction in space time from 4 h to 4.6 min compared to the case when only two capillary reactors (1/8 and 1/4 inch) were used. This represents an improvement of around 50 times in reactor performance. Compared to batch operation, space–time yield increased by 3 orders of magnitude. Kinetics of synthesis of [EMIM]$EtSO_4$ was reported in a millimeter range reactor (Gröbe-Böwing and Jess, 2005). The authors used a tubular reactor with an internal diameter of 4 mm. They modeled loop and multi-tubular reactors based on the kinetic parameters they evaluated and heat transfer correlations that have been reported. The authors reported an optimal recycle ratio value of 2.3. Suitability of using a loop reactor for synthesis of [EMIM]$EtSO_4$ was also reported by Willmes and Jess (Willmes and Jess 2013).

A millimeter-sized tubular reactor (with an internal diameter of 6 mm) was used to demonstrate the flow synthesis of [EMIM]$EtSO_4$ at a scale of 4 kg per day at 30°C (Gröbe-Böwing et al., 2007). The two incoming reactants were infused into the reactor tube, which was cooled externally. The authors reported that the reaction enthalpy is − 102 kJ/mol. They also reported that the reaction can only be controlled if the cooling temperature is 30°C or less. Any higher cooling temperature would lead to thermal runaway. In a previous work (Sen et al. 2016), we have compared space–time yield and rate of production for flow synthesis of [EMIM]$EtSO_4$ in 3 different designs of micro-reactors. CFD analysis

of the flow field was also reported. Serpentine micro-reactor was found to outperform the other two designs.

Numerical simulations are often been used to model reactive flows in micro-channels (Wang et al. 2011; Shin et al. 2013; Uriz et al. 2014; MacInnes 2002; Shao et al. 2010; Angeli et al. 2000). There are reports on CFD modeling of complex polymerization reactions in micro-channels also (Garg et al. 2015; Serra et al. 2007; Mandal et al. 2011). Such models provide valuable insights into the flow, temperature, and species concentration field across the entire micro-channels including the microfluidic junction.

In most previous studies on flow synthesis of ionic liquids, a multi-scale approach has been used. The incoming reactants are first brought into contact with each other in a micro-mixer, then passed through a micro-reactor, and finally into a millimeter-sized tubular reactor. Almost all authors have used some form of a micro-structured reactor or micro-mixer before injecting the reacting stream into a capillary. However, these micro-structured reactors and mixers require specialized manufacturing techniques and are expensive and not readily available. In this work, we focus on synthesis of $[EMIM]EtSO_4$ in a simple PTFE micro-capillary (diameters less than 1 mm). Micro-capillaries are arguably the cheapest available micro-channels. A simple Y-type microfluidic junction is used to mix the two incoming reactants. To the best of our knowledge, flow synthesis of $[EMIM]EtSO_4$ in a micro-capillary alone has not been previously reported. This represents the novelty of the present work. Effect of microfluidic mixing, reaction temperature, flow rate, and micro-capillary diameter on product yield has been systematically studied. A numerical model (COMSOL 5.3) of the reacting flow inside the micro-capillary has also been developed so as to obtain more insights into the transport processes and also to explain the experimentally observed trends. Furthermore, simulations have been used to understand how obstructions in an otherwise straight flow path can affect product yield.

2 Details on experimental procedure and numerical model

2.1 Chemicals

The reactants used in this study are diethyl-sulfate and 1-methylimidazole, both of which are of AR grade and purchased from Merck. No special pretreatment or purification is done before using them. 1-ethyl-3-methylimidazolium ethyl-sulfate IL (99%) is also purchased from Merck as a reference. The reaction is shown in Fig. 1. This reaction is a single-step reaction and is associated with a high degree of exothermicity.

2.2 Experimental setup

Figure 2 shows the schematics of the experimental setup. Two continuous flow syringe pump systems (flow rate in the range of 0.01–10 ml/min, New Era, NE 1010) infuse 1-methylimidazole and diethyl-sulfate to the microfluidic junction (fabricated by precise drilling in a 1 inch diameter polypropylene disk) at specified flow rates. A continuous flow syringe pump comprises of two syringe drivers working in a push–pull configuration. Each of these continuous flow systems take suction from a vessel containing the respective reactant. A micro-precise drill bit of 0.72 mm is used to drill cylindrical holes in the junction. The drill length is limited to 10 mm to ensure straight holes. The fabricated Y-junction used in the experiments is shown in Fig. 3. The two reactant streams are made to mix at the Y-junction and the mixed stream then flows into the attached micro-capillary. The micro-capillary essentially provides residence time required by the reaction. The micro-capillary is made of PTFE and is procured from Cole Parmer. Different diameters of such capillaries have been used in the experiment. The micro-capillary is connected to the microfluidic junction using externally threaded end connectors (6 mm, made of PFA). The microfluidic junction has a corresponding recess with internal threads which fits securely with the end connector. Leak proof fit is ensured using ETFE ferrules (Darwin Microfluidics make). The microfluidic junction along with the micro-capillary is kept inside a constant temperature water bath (IKA HB 10) to regulate the reaction temperature. The uniformity in temperature across the bath was better than 0.5°C. The micro-capillary outlet is placed inside a collection vial which is kept in an ice bath so as to thermally quench the reaction. The residence/contact time is kept fixed at 40 s in all the experiments. Micro-capillary of different lengths (0.25–2 m, please refer to Table 2) have been used to study the effect of flow velocity on yield. In doing so, the residence time is always held fixed at 40 s, while the flow rate (hence velocity) is varied. The molar ratio of the two reactant streams is kept at unity. In the experiments conducted to study the effect of velocity (0.00618–0.0494 m/s, please refer to Table 2) and tube diameter (300–1000 µm, please refer to Table 2) on conversion, reaction temperature is held fixed at 50^0C. Additional experiments are also carried

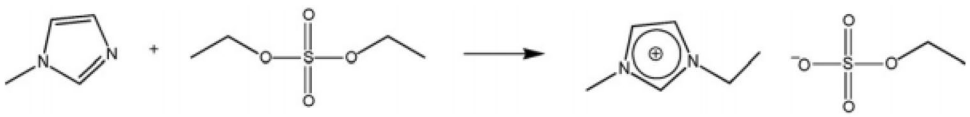

Fig. 1 Alkylation reaction for synthesis of $[EMIM]EtSO_4$

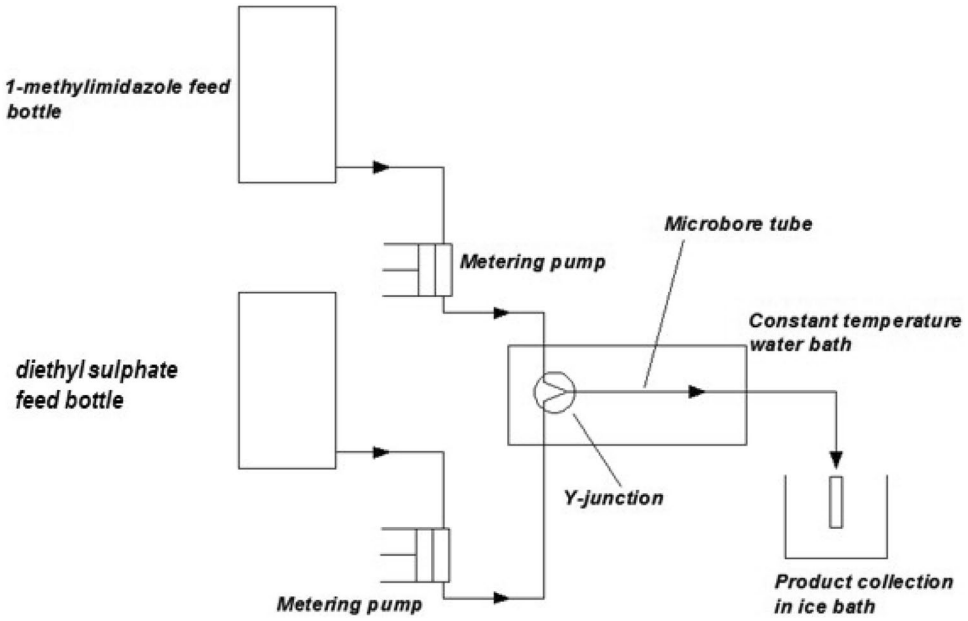

Fig. 2 Schematic of the experimental setup

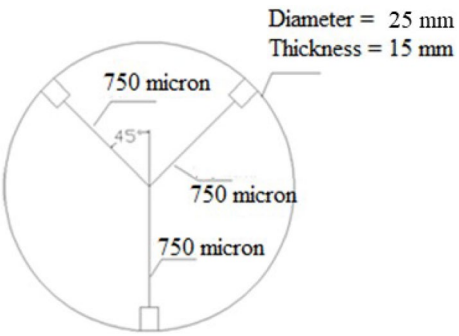

Fig. 3 Schematic diagram of the Y-microfluidic junction drilled in a PP disk (15 mm thick)

out to determine effect of reaction temperature. All reactor temperature mentioned in the work essentially refers to the bath temperature. The wall thickness of the capillaries used was ~ 0.25 mm. Though thermal conductivity for PTFE is quite low, such low values of wall thickness essentially mean that the actual temperature inside the PTFE micro-capillary will be very close (if not same) to that inside the bath.

Pressure drop across the micro-capillary was measured experimentally using an inline digital pressure gage (0–4 bar range, resolution of 0.05 bar) for some experiments (effect of reaction temperature). The maximum pressure drop encountered in this work was around 0.85 bar.

2.3 Product analysis

The product ionic liquid (IL) conducts electricity because it is in an ionic state. When a fixed volume of the product sample is mixed with a fixed volume of ethanol, the electrical conductivity of the sample is solely due to the presence of the IL (ethanol is not conductive). In fact, the conductivity value will clearly depend on the concentration of IL mixed in the ethanol. First, we prepare a calibration plot by mixing measured and predetermined volumes of pure [EMIM] $EtSO_4$ (99%, Merck) in a fixed volume of ethanol (50 mL) and measuring its conductivity. This calibration plot is then used to measure the concentration of IL in the reactor effluent. The effluent from the micro-reactor is analyzed using this calibration plot. We take 250 µL of reactor effluent and mix it with 50 mL of ethanol and measure the conductivity. Care is taken to ensure that the measurement temperature is kept the same as that used for preparing the calibration plot (~ 25 °C). The product yield can be directly obtained from this measured electrical conductivity data along with the calibration plot.

Product yield (Yd) is defined as the number of moles of the ionic liquid formed per unit mole of 1-methylimidazole consumed. The product is also characterized by proton NMR (supporting information, Fig. S1).

Apart from product yield, production rate is calculated from Eq. (1) given below

$$PR = \frac{24 \times 60 \times \rho_{MIM} \times q_{MIIM} \times Y_d \times MW_{IL}}{MW_{MIM}}, \quad (1)$$

where PR is production rate in g/day, q_{MIM} is flow rate of 1-methylimidazole in mL/min, ρ_{MIM} is density of 1-methylimidazole (1.035 g/mL), MW_{IL} is molecular weight of ionic liquid (236.29 g/gmol), and MW_{MIM} is molecular weight of 1-methylimidazole (82.1 g/gmol). PR essentially shows

the quantity of material that can be produced on continuous usage of the reactor.

In Eq. (1), Yd is fractional product yield (−) which is obtained from the ratio of the measured conductivity value to the slope of the calibration curve.

Another parameter of interest is space–time yield (STY) which essentially shows the specific performance of the reactor. This term is defined as per Eq. (2)

$$STY = \frac{PR}{24 \times 60 \times V_R}, \tag{2}$$

where STY is space–time yield in g/min-L, V_R is reactor volume in L.

2.4 Governing equations

Numerical simulations for the microfluidic system used in this work (Y micro-junction followed by micro-capillary) are reported in this section. Due to small diameters involved, flow in microfluidic junctions and in micro-capillary is essentially laminar. The flow filed has been obtained by solving the classical Navier–Stokes equations. Species and energy transport equations have also been solved along with the Navier–Stokes equations. The velocity field goes as the input for the solution of energy and species transport equations. As a reactive flow is being modeled, source terms (positive for products and negative for reactants) are included the species transport equations (one equation for each of the components involved in the reaction). As the reaction considered is exothermic, a corresponding source term for the heat of reaction is also included in the energy transport equation. Equations (3–8) show the governing equations used. A commercial finite element-based solver COMSOL Multiphysics 5.3 has been used for simulations.

$$\nabla.\overline{\mathrm{U}} = 0, \tag{3}$$

$$\rho \frac{\partial \overline{\mathrm{U}}}{\partial \mathrm{t}} + \rho(\overline{\mathrm{U}}.\nabla)\overline{\mathrm{U}} = \nabla.[-\mathrm{p}\bar{\bar{\mathrm{I}}} + \mu(\nabla\overline{\mathrm{U}} + \nabla\overline{\mathrm{U}}^{\mathrm{T}})], \tag{4}$$

$$\frac{\partial \mathrm{C}_i}{\partial \mathrm{t}} + \nabla.\left(\overline{\mathrm{U}}\mathrm{C}_i\right) + \nabla.[-\mathrm{D}_\mathrm{i}\nabla\mathrm{C}_i] = \mathrm{R}_\mathrm{i}, \tag{5}$$

$$\rho C_p \frac{\partial \mathrm{T}}{\partial \mathrm{t}} + \nabla.[-k\nabla T + \rho C_p T\overline{\mathrm{U}}] = (-\mathrm{H}_\mathrm{i})\mathrm{R}_\mathrm{i}. \tag{6}$$

$\overline{\mathrm{U}}$, k, C_p, ρ, and μ, are the velocity vector, thermal conductivity, density, and viscosity of the reaction mixture, respectively. The reaction mixture's physical properties have been taken as concentration weighted average of the participating species as shown in Eq. (7) below.

$$\varphi_{\mathrm{mix}} = \frac{\sum_{\mathrm{i}=1}^{n} \mathrm{C}_i\varphi_i}{\sum_{i=1}^{n} \mathrm{C}_\mathrm{i}}, \tag{7}$$

where φ_{mix} is the average physical property of the reaction mixture, C_i and φ_i are the concentration and physical property of the i^{th} species and n is the number of species. Hence, physical properties of the system vary across the computational domain. By defining the physical properties as dependent on concentration the above set of equations becomes completely coupled. R_i and C_i are the rate of formation/consumption and concentration of \textit{i} th chemical species. H is the enthalpy/reaction heat of the reaction considered. The rate of consumption or generation of a particular species involved in a reaction is related to the rate of reaction (R_r) by stoichiometry of that species in the reaction. The reaction rate of defined according to Arrhenius expression (Eq. (8)).

$$R_r = k_0 e^{-\left(\frac{E_a}{RT}\right)} C_1 C_2, \tag{8}$$

where k_0 is the pre-exponential/frequency factor and E_a is activation energy of the reaction. Values for k_0 and E_a are 1.28×10^9 m^3/mol-s and 89 kJ/mol, respectively (Böwing and Jess 2007) C_1 and C_2 being the reactant concentration (reactants being 1-methylimidazole and diethyl-sulfate, respectively). Table 1 mentions values of the physical properties of the individual reactants, i.e., 1-methylimidazole and diethyl-sulfate (NIST Web Book) and product, i.e., [EMIM] $EtSO_4$ (Zhang et al. 2006) as used in the simulations. Physical properties of individual components are considered as constant and are their temperature dependency is neglected.

Though coupling of physical properties of the reacting system with respect to concentration is implemented in the model, effect of temperature.

A picture of the computational domain is shown in Fig. 4(a) later in Sect. 4. A velocity boundary condition is defined at the inlet of the two reactants while a pressure outlet boundary condition is defined at the exit of the micro-capillary. Results of grid independence test and validation of CFD model with respect to analytically determined pressrue drop (discussed later in Sect. 4) are also shown.

Table 1 Values of physical properties of reactants and products used in simulation

	1-methylimidazole	diethyl-sulfate	[EMIM]$EtSO_4$
ρ (kg/m^3)	1035.02	1179.50	1240.12
C_p (J/kg-K)	132.72	162.2	11.01
μ (Pa.s)	0.00159	0.00179	0.0022348
k (W/m–K)	0.185		

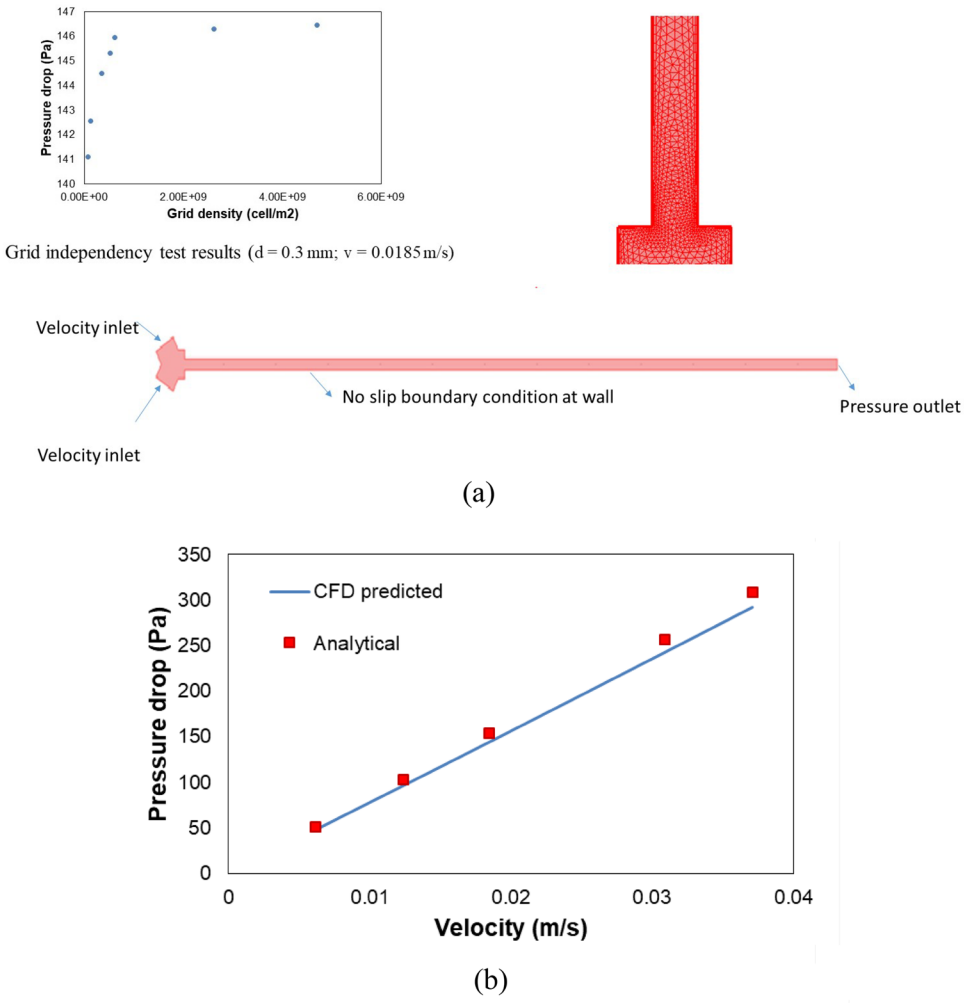

Fig. 4 **a** Grid independency test, snapshot of meshed computational domain and boundary conditions used in the numerical simulations and **b** comparison of CFD predicted pressure drop vis-à-vis analytical pressure drop

Table 2 Values of different parameters used in this work (residence time = 40 s)

Flow velocity (m/s)	6.18×10^{-3}	1.24×10^{-2}	1.85×10^{-2}	3.09×10^{-2}	4.94×10^{-2}
a) Flow velocity					
Length (m)	0.25	0.50	0.75	1.25	2
Re (-)	1.85	3.72	5.55	9.27	14.8
Micro-capillary inner diameter (μm)	300				
Temperature (°C)	50				
Micro-capillary inner diameter (μm)	300	500	800	1000	
b) Diameter of micro-capillary					
Length (m)	1.234				
Temperature (^{0}C)	50				
Flow velocity (m/s)	3.09×10^{-2}				
Temperature (^{0}C)	50	60	70	80	90
c) Temperature					
Length (m)	1.234				
Micro-capillary inner diameter (μm)	300				
Flow velocity (m/s)	3.09×10^{-2}				

3 Experimental results and discussion

The alkylation reaction studied here occurs in a single phase. However, it is important to ensure that the two reactant streams are well mixed to generate a completely homogeneous mixture. Table 1 shows the parameters whose effect on yield of the product, production rate, and space–time yield has been studied. When one parameter is varied, others are kept constant at base values highlighted in bold in Table 2. In all experiments, the residence/contact time is held fixed at 40 s. While studying the effect of velocity, tube lengths are changed to keep the residence time same. For all cases, values of Reynolds number ($Re = dV\rho/\mu$) are also shown. d is the micro-channel diameter, V is flow velocity, ρ and μ are density and viscosity of reacting system.

3.1 Influence of flow velocity

The velocity of the fluid flowing through a junction has a direct impact on the degree of mixing at the junction. The velocity is defined as the ratio of the total volumetric flow rate to the cross-sectional area of the tube. The higher the velocity, the greater the degree of mixing at the junction.

In a typical Y-junction, at lower flow velocities, the two incoming reactants will flow parallel to each other without mixing (Sarkar et al. 2014). The mixing of the reactants is purely due to molecular diffusion, which is a very slow process. As the flow velocities increase, a vortex regime is created, where secondary currents are generated within each reactant stream. This leads to surface replenishment at the interface, which increases mixing to some extent. However, the basic mechanism of mass transport is still dominated by molecular diffusion. On further increasing the flow velocity, an engulfment regime sets in, causing one stream to penetrate into the other. This drastically increases the mixing (Capretto et al. 2011; Engler et al. 2004). Hence, an increase in flow velocity is expected to increase the mixing amongst the two incoming reactants leading to an increase in product yield. Another crucial parameter for reactive flow through micro-capillaries is development of thermal boundary layer. For laminar flow through a cylindrical pipe, thermal boundary layer thickness at a given axial distance decreases with an increase in Peclet number (Barozzi and Pagliarini 1985). Hence, a reduction in thermal boundary layer thickness at a given axial distance is expected if flow velocity is increased. This essentially means that it will take a longer time for the fluid inside the micro-capillary to reach wall temperature. In the case of a reacting system, this means that an increase in flow velocity will decrease product yield.

Figure 5(a) shows that with an increase in flow velocity, product yield first increases, reaches a maximum, and then starts to fall. All five data points have been repeated three times each so as to ensure the reliability of the experimental measurements. Overall coefficient of variance (of repeatability measurements) is found to be 6.26%. If mixing were the only factor affecting yield, then yield would increase continuously with increasing velocity, as mixing is known to improve with increasing velocity. The maximum yield value in Fig. 5(a) at a critical flow velocity indicates that two opposing factors are affecting the yield. At flow velocities below this value, the increase in yield due to enhanced mixing outweighs the decrease in yield due to a reduction in thermal boundary layer thickness. As a result, there is an overall increase in yield. Beyond the critical velocity, the opposite is true. The decrease in yield due to a decreasing thermal boundary layer outweighs the increase in yield due to enhanced mixing. As a result, there is an overall decrease in yield beyond the critical velocity. Effect of flow velocity on mixing and thermal boundary later will be explained using numerical simulations later in Sect. 4

Figure 5(b) and (c) shows how production rate (PR) and space–time yield (STY) change with flow velocity. PR increases with increasing velocity until the critical velocity, after which it plateaus. This is because yield (Yd) decreases after the critical velocity. However, the continuous increase in the 1-methylimidazole flow rate offsets the decrease in Yd, so PR does not decrease but becomes more or constant after critical value. In terms of specific reactor performance, STY reaches a maximum at the critical velocity. STY is as high as 1164.43 g/min-L at a critical velocity of 0.0185 m/s. Thereafter, STY decreases and then slowly starts to rise again due to the increase in values of PR.

It is important to note that the tube length was also increased concurrently as the flow velocity was increased to keep the residence time constant at 40 s. The tube length was increased from 0.25 m to 2 m. The simultaneous increase in flow velocity and micro-capillary length led to a corresponding increase in pressure drop from 0.025 bar to 0.85 bar.

3.2 Influence of reaction temperature

Figure 6(a) shows the influence of reaction/reactor temperature on product yield. In Fig. 6, all parameters except reaction temperature are held constant (i.e., flow rate, tube diameter, and length). It is noted that yield increases monotonically with an increase in temperature for a given velocity and residence time. In fact as the temperature is increased from 40^0C to 80 ^{0}C, the yield increases by a factor of 1.6. This is to be expected, as an increase in reaction temperature will increase the rate of the reaction. The fact that the yield increases monotonically with increasing temperature indicates that at a flow velocity of 3.09×10^{-2} m/s, mixing is no longer a significant factor limiting the overall reaction.

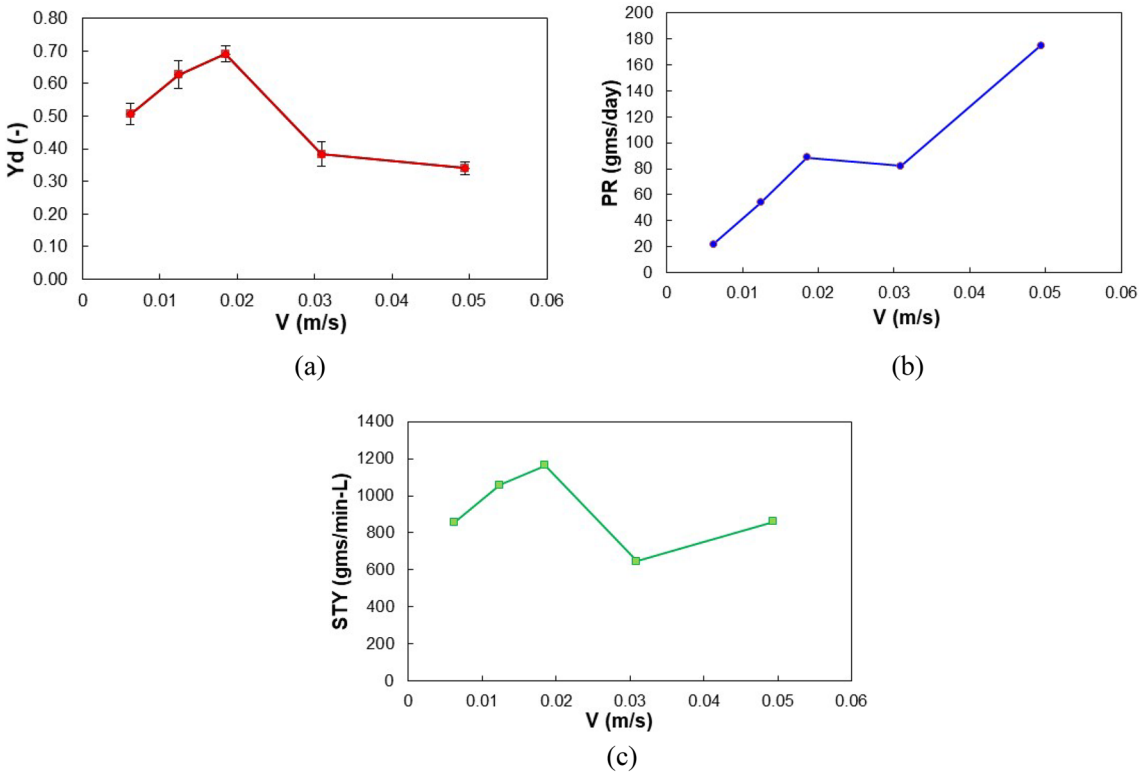

Fig. 5 Influence of flow velocity on **a** product yield; **b** production rate; **c** space–time yield (T = 50^{0}C; d = 300 μm; τ = 40 s; length of micro-capillary used are 0.25, 0.5, 0.75, 1.25, and 2 m for lowest to highest flow velocity, respectively)

Instead, the reaction kinetics is the main factor limiting the process.

Figure 6(b) and (c) shows corresponding influence of reaction/reactor temperature on production rate (PR) as well as space–time yield (STY). Both these parameters (i.e., PR and STY) are seen to increase with a rise in reaction temperature. The trends of PR and STY closely follows the experimental trend of product yield (Yd) because the only variable that is changing in definition of PR and STY is yield. It may be mentioned that the highest value of STY reported in this work (1258.4 g/min-L) is achieved at a reaction/reactor temperature of 80 ^{0}C in a 300 μm diameter micro-capillary at a flow velocity of 0.0309 m/s.

3.3 Influence of diameter of micro-capillary

Figure 7(a) shows the influence of diameter of the micro-capillary tube on the product yield. It is noted that the product yield decreases monotonically with an increase in micro-capillary diameter. The thermal boundary layer takes longer to develop as the micro-capillary diameter increases, while the velocity and reaction temperature remain constant. This means that the thermal entrance effect is longer. Thus for tubes of larger diameter, it would take a significant tube length before the center of the tube attains the skin temperature. Hence, the average temperature and consequently the rate of reaction will be low in the initial lengths of the micro-capillary. On an overall basis, this causes yield to reduce with increasing tube diameter. Similar phenomenon has been observed for macro-scale reactors in which increase in reactor diameter is found to reduce the conversion (Goswami et al. 2014).

Figure 7(b) and (c) shows the corresponding effect of micro-capillary diameter on production rate (PR) and space–time yield (STY). A monotonic rise in PR is noticed as micro-capillary diameter is raised from 300 to 1000 micron. In fact PR is as high as 930 g/day for a tube diameter of 1 mm. This is because with an increment in tube diameter, flow rate of 1-methylimidazole is increased from 0.05 to 0.55 mL/min to keep residence time fixed at 40 s. This essentially leads to a significant increase in PR according to Eq. (1). However, with increase in tube diameter, reactor volume (V_R) also increases which essentially means that in terms of specific performance, the reactor performs poorly. This is clearly represented in Fig. 7(c) where STY is seen to reduce with increase in diameter of micro-capillary.

It is, therefore, observed that mixing as well as heat transfer are of primary importance in the range of variables studied in this work. In the following section, we report

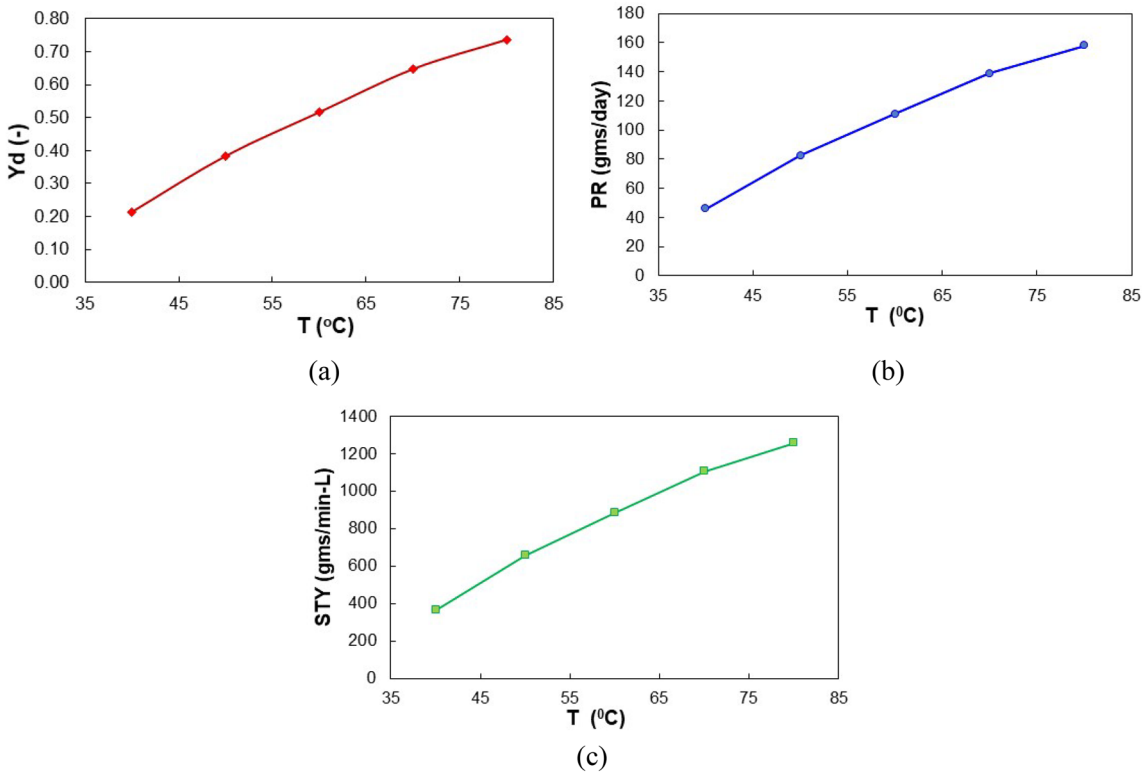

Fig. 6 Influence of reaction/reactor temperature on **a** product yield; **b** production rate; **c** space–time yield (d = 300 μm; $v = 3.09 \times 10^{-2}$ m/s; $\tau = 40$ s)

numerical simulations for this reactive system to explain the experimental trends given above.

4 Numerical modeling of reactive flow system

4.1 Grid independency test and model validation

An unstructured mesh have been used in the simulations. A boundary layer is used to refine the mesh near the wall of the micro-channel. A mesh density of 6.23×10^8 cells/m^2 has been used in the present work based on the results of a grid independency test carried out for a geometry featuring the Y-junction and a 300 μm micro-channel. Details of the grid independency test along with a snapshot of the meshed domain are shown in Fig. 4(a). Figure 4(a) also shows the boundary conditions used in the simulations.

A 2D model of the microfluidic junctions along with a small section of the attached micro-capillary have been used in the simulations. A 2D modeling approach is selected to reduce computational resources required for the simulations. Though a 3D approach would have provided more information (cross-sectional) on the flow field but for reactive systems in micro-channels (polymerization), it has been reported (Serra et al. 2007) that result obtained from a simple 2D model matches reasonably well with those from a detailed 3D model. The tube length used in the simulations is much smaller than the tube lengths used in the actual experiments. This is done to keep the computational requirements within reasonable limits. Maximum length of the tube used in simulations is 0.030 m, whereas the maximum length used in experiments is as high as 2 m. Hence, the numerical simulations cannot be used to reproduce the experimental results. The purpose of the numerical simulations is to understand how the flow and thermal fields are affected with variation in flow velocity, tube diameter, and temperature, and to substantiate the experimental trends.

Though no attempt is made to quantitatively compare CFD predicted yields with experimental values we have compared the pressure drop predicted by the CFD model against pressure drop obtained using analytical expression for flow in a micro-capillary under laminar flow conditions (Hagen–Poiseuille equation). A set of simulations are carried out for different flow rates in a 300 micron diameter tube 30 mm long. The congruence between the CFD predicted results and the analytical results is very good (even for a 2D model) as can clearly be seen in Fig. 4(b). This shows that the developed 2D CFD model is able to predict the hydrodynamics inside the micro-capillary quite well. Conversion

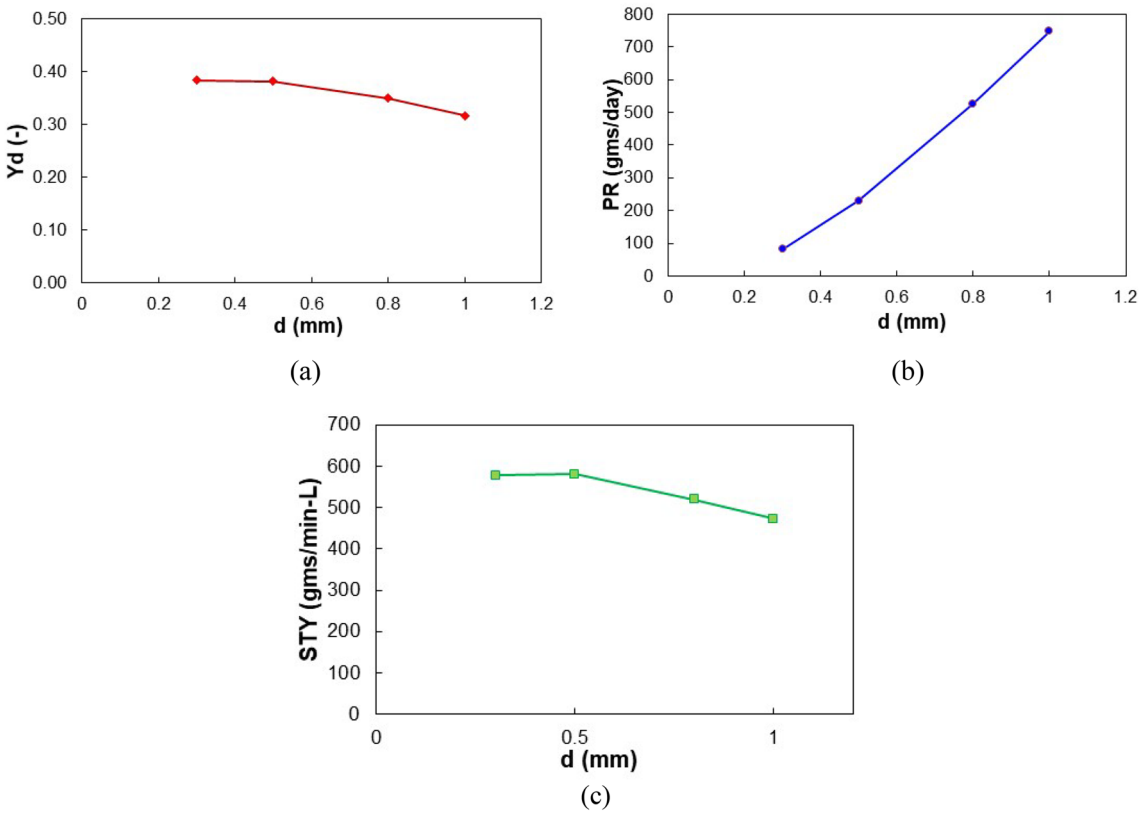

Fig. 7 Influence of micro-capillary diameter on **a** product yield; **b** production rate; **c** space–time yield ($T = 50\ ^0C$; $v = 3.09 \times 10^{-2}$ m/sec; $\tau = 40$ s)

(for a known kinetics) as well as heat transfer characteristics is closely linked to the hydrodynamics inside the capillary. Hence, if the CFD can predict the hydrodynamics accurately, it may be said that CFD prediction on product yield will also be reasonably accurate.

4.2 CFD predicted results

Figure 8(a–c) shows the effect of temperature, flow velocity, and micro-capillary diameter on the yield, as predicted from the CFD model, at the outlets of the micro-reactor.

Figure 8(a) shows that as the temperature is increased, the product yield increases monotonically. The same has been observed in the experiments. Hence, predictions of the numerical model are in line with experimental observations. It is observed that the typical values of yield at reactor outlet are very small. This is due to the fact that the length of the micro-capillary used in numerical simulations is significantly smaller than that used in experiments so as to keep the computational resources within reasonable limits.

Figure 8(b) shows the effect of the flow velocity on the product yield at the outlet. In all the simulations carried out, the residence time is kept constant at 0.81 s, length of the tube section modeled is varied accordingly. It may be mentioned that the choice of residence time at 0.81 s is rather ad hoc. The main driving force for choice of this residence time was to ensure that the length of the micro-capillary is not too large which would otherwise have increased the computational time.

It is observed that with an increase in flow velocity, the product yield initially increases, reaches a maxima, and then slightly decreases. This is in line with the experimental trends. This is because with an increase in flow velocity initially mixing is enhanced which tends to increase the yield. However with further increase in velocity, development of a thermal boundary layer is delayed which leads to a reduced conversion. Figure 9(a) shows the variation of temperature profiles of the reaction mixture in the Y-junction and micro-capillary for different flow velocities. It is observed that as the flow velocity is increased the temperature inside the microfluidic junction and in the initial length of the micro-capillary comes down. This indicates that at higher velocity, it takes longer distance for the reaction mixture to feel the skin temperature.

Figure 8(c) shows a decrease in the product yield as the micro-capillary diameter is increasing. This is in agreement with experimental observations. Figure 9(b) shows the temperature profiles for micro-capillary of three different

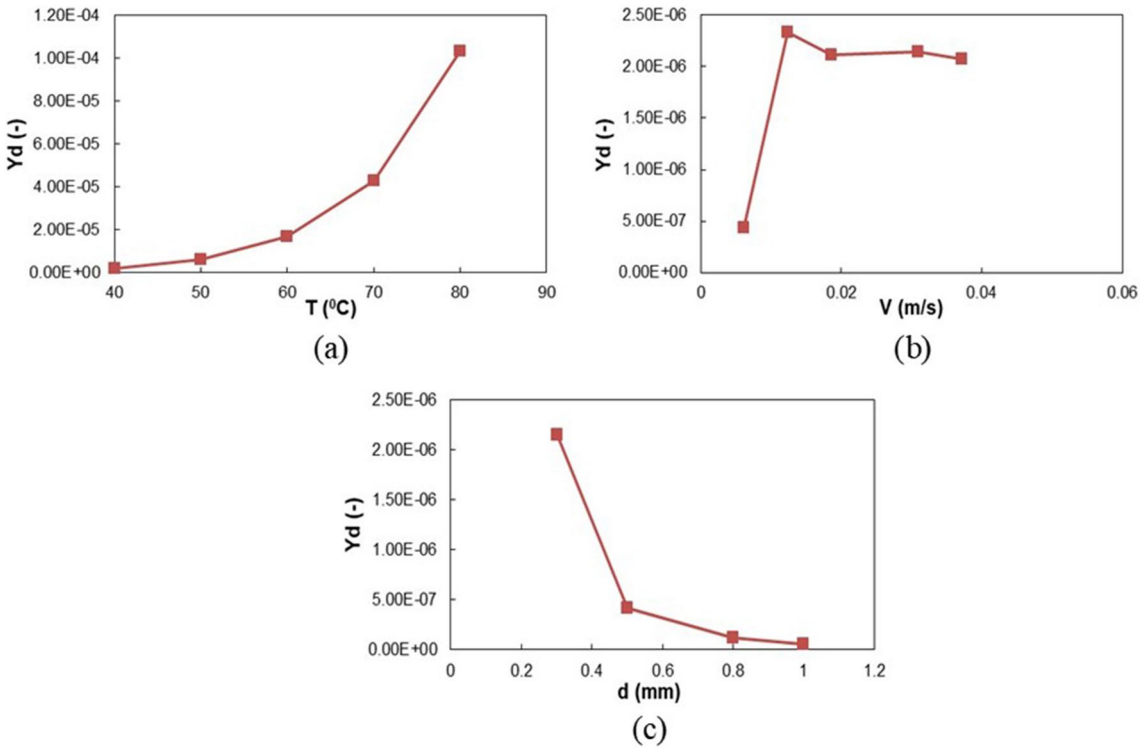

Fig. 8 Effect of **a** reaction temperature (d = 300 μm; $v = 3.09 \times 10^{-2}$ m/s; τ = 0.809 s), **b** flow velocity (d = 300 μm; T = 40 ^{0}C, τ = 0.809 s) and **c** micro-capillary diameter (T = 40 C; $v = 3.09 \times 10^{-2}$ m/s; τ = 0.809 s) on the yield for the microreactors having Y-type microfluidic junctions as obtained from numerical simulations

diameters. Figure 9(b) shows that as the micro-capillary diameter is increased, the development of the thermal boundary layer is delayed. For a large diameter tube, temperature can be significantly lower in the entrance zone. The reaction rate decreases with increasing micro-capillary diameter, and the final product yield at the outlet is reduced as a result. The predictions from the numerical simulations, thus, corroborate the experimental trend of effect of micro-capillary diameter on yield. and explanation of this trend as given in the previous section.

4.3 Effect of flow obstacles

It is known and documented that mixing in T-junction and Y-junction micro-channels with straight layout is rather poor (Engler et al. 2004; Capretto et al. 2011; Sarkar et al 2014) at low Reynolds number. After the microfluidic junction, the two streams flow parallel to each other in the straight tubes and the mixing is purely diffusive in nature (Re < 10). There are several possible methods to enhance mixing. Introduction of obstacles in the flow path is one of the methods to enhance the mixing (Fang et al. 2012; Alam and Kim 2012; Sarkar et al. 2014). In a channel having obstacles in the flow path, the streams will flow around the obstacles leading to strong lateral flow velocity components. These will lead to significant cross-flow (chaotic advection based) mixing of the reactant streams. A greater degree of lateral flow components will also lead to a greater degree of homogenization of the temperature field leading to short thermal entrance effects. Because of these two factors, micro-channels with obstacles in flow path should have much better performance than the micro-channels without obstacles. Superior performance of the micro-channels having periodic obstacles (mixing units) has been demonstrated experimentally. Bhagat et al. 2007 have reported that micro-channels with diamond-shaped, circular, and triangular flow obstacles provide better mixing than straight channels. Fang et al., 2011 demonstrated the use of a periodic mixing element to significantly enhance mixing. The studies involving micro-channels with obstacles in flow path reported so far are, however, focused on the effects of presence of obstacles on mixing. In the present study, we have gone a step beyond to evaluate, using numerical simulations, the effect of the presence of such obstacles in the flow path on product yield. In addition to the designs already reported, a micro-channel having triangular obstacles arranged in staggered fashion is also evaluated. At this stage, it must be clarified that the results mentioned below are those predicted by the numerical model. In this work, we did not physically fabricate such 2D obstacles inside the micro-channel. However,

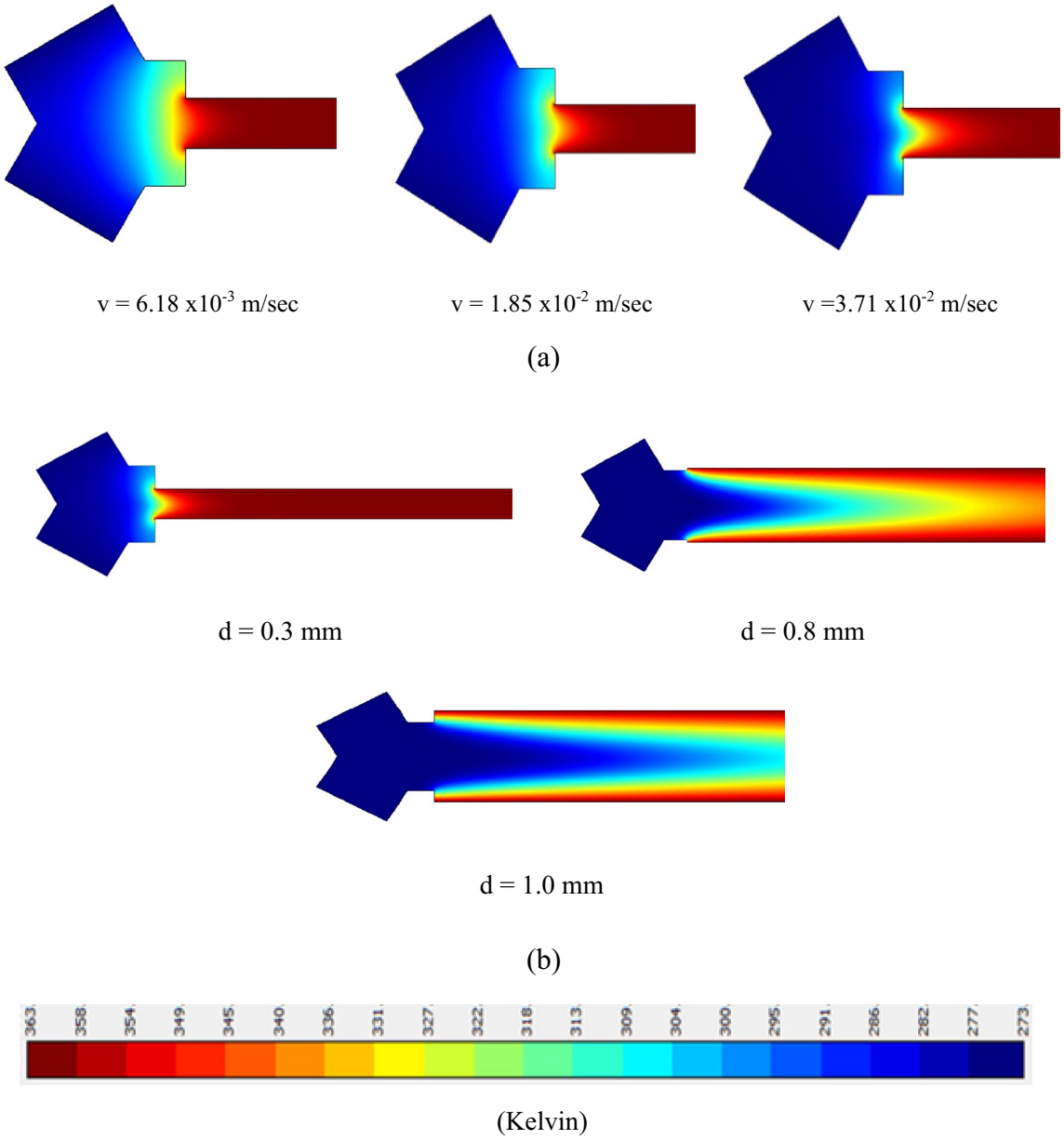

Fig. 9 Temperature field at **a** three different flow velocities (T = 90 ^{0}C; d = 0.3 mm; τ = 0.809 s) and **b** three different tube diameter (T = 90 ^{0}C; τ = 0.809 s; v = 0.00309 m/sec) for Y-microfluidic junction. The color bar is in Kelvin (

such obstacles can be fabricated in a straight micro-channel prepared on a chip (e.g., etched in glass or a PDMS chip).

Figure 10 shows the micro-channels having periodic mixing elements/obstacles that have been evaluated numerically. It may be noted for all cases, the microfluidic junction was the same (i.e., Y-junction).

Figure 11(a) shows the variation of product yield with velocity for the four different micro-channel designs. It can be seen that all the designs with obstacles lead to higher product yield than the design without obstacles (i.e., simple Y mixer with straight channel). This is clearly attributed to superior mixing due to obstacles in the flow path. In all the simulations carried out the residence time has been kept constant at 0.809 s.

Another interesting trend that is observed is that the product yield tends to increase with increase in velocity especially at lower ranges of flow velocity. In fact for designs 1, 3 and to an extent even for design 2, a maxima in product yield is seen. While the fall in yield is attributed to an extended thermal entrance effect at higher velocities, the initial rise at low velocities is attributed to an increase in mixing as velocity is increased. Flow obstacles divert the flow laterally in the longitudinal plane of the micro-channel. These radial components of the flow essentially lead to chaotic

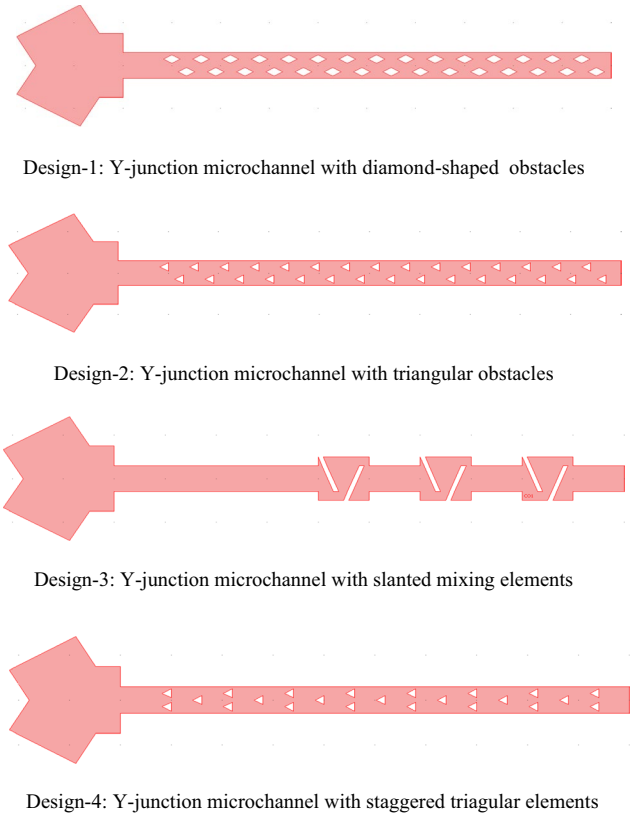

Fig. 10 Different micro-channels with obstacles evaluated by carrying out numerical simulations

advection in these channels because of which the interface between the two incoming reactant streams gets stretched and smeared which significantly increase mixing of one stream into another.

Figure 11 (b) depicts CFD predicted pressure drops for all the different designs. It can be seen that compared to a straight channel there is a significant increase in pressure drop in all geometries with obstacles. This is expected because the lateral currents which are responsible for creating better mixing of the incoming reactants come at the expense of additional energy which is represented in terms of higher pressure drop. A comparison reveals that pressure drop in designs 3 and 4 are relatively higher than that in design 1. The highly torturous flow path created by obstacles in design 3 is responsible for the higher pressure drop encountered in this design. On the contrary, pressure drop encountered in design 1 is quite less (in fact the least amongst all designs) due to the streamlined flow generated by diamond-shaped obstacles. Hence, design 1 is clearly the optimal design of obstacles that provide highest product yield (Fig. 11a) at a reasonable expense of pressure energy.

Among all the designs having obstacles in the flow path, performance of the design 1 (diamond-shaped obstacles) is found to be the best. This is followed by the design 2 (triangular shaped obstacles). Performance of design 4 is the worst amongst all the designs. These differences can be attributed to the enhancement of the contact area between the two reactant streams and effective reactor volume. As discussed earlier in the range of Reynolds number studied in this work, the two incoming reactant streams do not penetrate into one another and flow parallel to each other. Inside the channel presence of the flow barrier will force the streams to move in a zigzag manner and in doing so will increase the effective contact area of the two leading to higher conversions. Figure 12 (a) and (b) shows the product concentration contour and effective interface between two incoming reagent streams for the micro-channels with obstacles, respectively. An interesting observation in Fig. 12 (a) is that for design 3, there is a region where the product yield is significantly higher on the leeward side of the slanted barriers. This is because the fluid entrapped in that region is not replenished by the main stream. As this pocket of fluid is isolated from the main fluid flow, the effective reactor volume

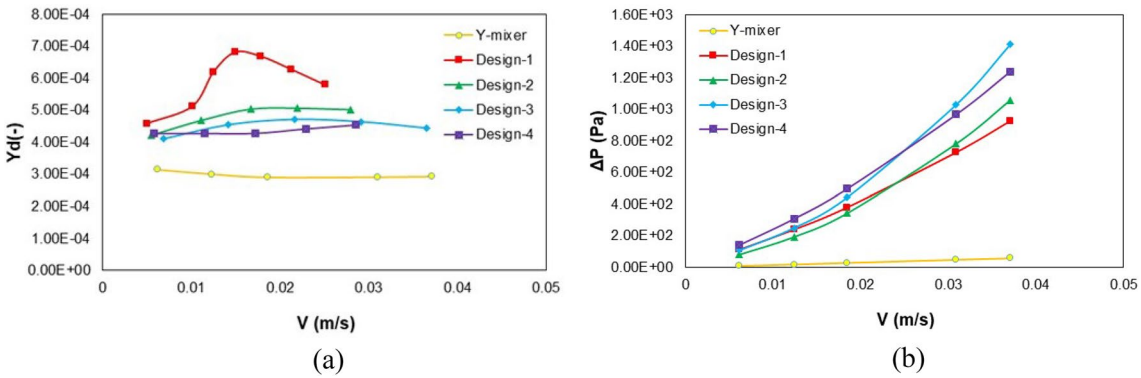

Fig. 11 Effect of flow velocity on **a** product concentration and **b** channel pressure drop for different designs of micro-channels having obstacles in flow path ($\tau = 0.809$ s; $T = 90.^{0}C$)

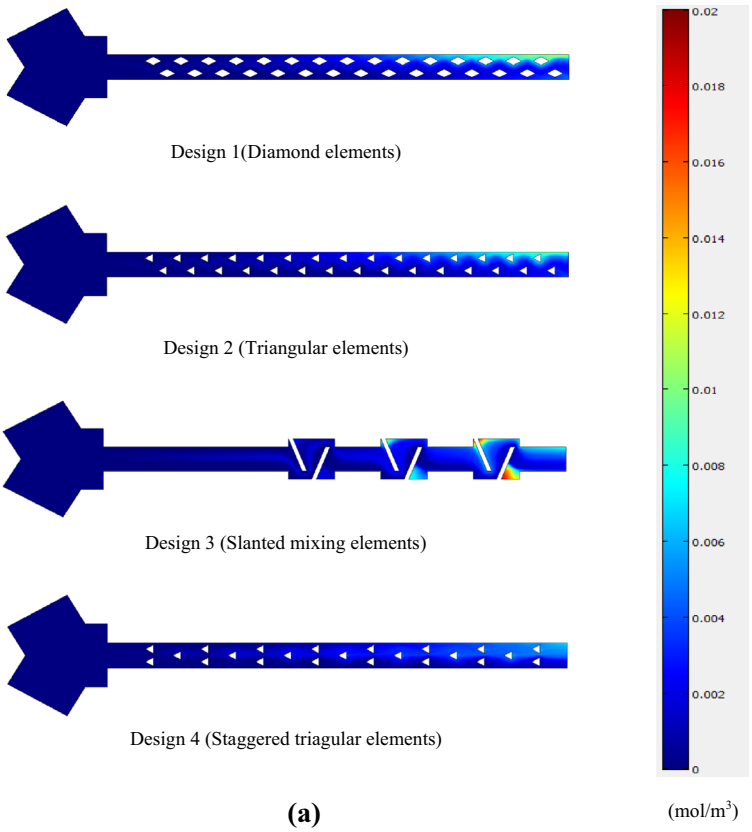

Fig. 12 **a** Product concentration contour (color bar in mol/m^3) and **b** interface between the two incoming reagent streams for different obstructed micro-channel layout studied ($\tau = 0.809$ s; T = 90.°C) (color figure online)

is reduced which leads to reduced product yield at the reactor outlet. This reduction in effective reactor volume which translates into a reduction in residence time (for the same reactor, length and velocity) overcomes the improvement in contact area between the two incoming streams afforded by design 3 (in comparison to design 1 and 2) and as a whole performance of design 3 reduces.

Figure 12(b) shows that the effective contact area (interface between the red and blue regions shown) generated by design 4 is less than that of designs 1 and 2 which leads to its poor performance. Quantitatively for a reactor length of 0.005 m (as in Fig. 12(b)), there are 15 crests both for designs 1 and 2; while for design 4, there are only 7. For these designs, the height of the crests are similar. Even though design 3 has only three crests for the same length, their height (and, thus, area) is significantly higher than others. As is observed in Fig. 12 (b), the effective contact area generated by design 1 and design 2 are not that different. Figure 13 shows the streamlines for design 1 and design 2. It can be seen that in design 1, the flow is squeezed or focused (compact streamlines) in between the diamond-shaped obstacles, while the flow is relatively more diffused in design 2. This is because the streamlines have a large area to flow in design 2 (regions at the windward side of the triangular obstacles); whereas in design 1, the flow area is constrained. This effect leads to a higher rate of surface renewal at the interface for design 1 which may be attributed to the better performance of design 1.

5 Possibilities of scale-up

The work reported proves the feasibility of continuous, solvent-free flow synthesis of [EMIM]$EtSO_4$ ionic liquids in a simple, flexible, and cost effective micro-capillary. Operating at an optimal flow velocity of 0.0185 m/s as identified in this work, it is possible to attain complete conversion of 1-methylimidazole by increasing the tube length (effectively increasing the residence time). However, production rate for a single such 300 micron diameter micro-capillary will be limited (order of 100 s of grams per day). For pilot/commercial-scale production rate, it is important to scale up. One of the major advantages of a micro-reactor system is its ability to be scaled up using a numbering-up approach. In this approach, the performance of a single micro-capillary is retained, while production is scaled up using a multitude of such micro-capillaries. This requires design of an optimal microfluidic header/distributor where in each of the two reactants are spitted and injected into each of the micro-capillaries. The challenge here in is to ensure the distribution of reactants into each capillary is as uniform as possible. In recent years, there has been some progress in this aspect. Table 3 below lists down the recent advances made in this filed.

Thus, it will be possible to scale up production rate to 8–20 times of what can be achieved in a single 300 micron micro-capillary reported here. This indeed will go a long way in establishing a numbered-up micro-capillary-based reactor system as a viable technology for pilot/commercial-scale production of speciality chemicals like ionic liquids.

6 Conclusion

Flow synthesis of ionic liquid [EMIM]$EtSO_4$ in a simple PTFE micro-capillary is reported for the first time. A Y-junctions serves as the microfluidic junction. Effects of velocity, reaction temperature, micro-capillary diameter on product yield, space–time yield, and production rate are studied. Product yield increases with increase in reaction/reactor temperature and reduces with an increase in micro-capillary diameter. With an increase in velocity, there is an increase in product yield initially till a critical velocity and then yield reduces with any further increase in velocity. This trend of variation of yield with velocity is attributed to two counteracting factors—enhancement of mixing with increase in velocity and reduction of temperature in the entrance zone with increase in velocity. Production rate keeps on increasing with increase in flow velocity, reaction temperature as well as micro-capillary diameter. An increase in production rate with increase in velocity and tube diameter is because

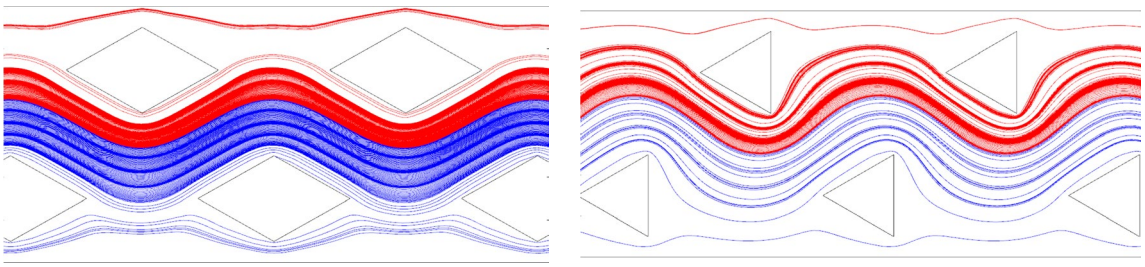

Fig. 13 Streamlines for two different layouts studied in this work ($\tau = 2.3$ s; T = 90.°C)

Table 3 xxxx

Reference	Scale-up factor	Scale-up technique	Remarks
Kashid et al. (2010)	6	External numbering-up. Two incoming reactants streams are split into 6 sub streams each and each set of sub streams a Y-shaped mixing element	The flow regime for all 6 micro-channels was the same as the case of a single channel Mass transfer rates were seen to increase with increase in velocity and in the presence of surfactants
Kockmann et al. (2011)	-	Plate-frame type modular reactor (chip based) (Lonza Plate Micro-reactor) which can be stacked up to any desired capacity	The authors demonstrated the viability of the stacked up micro-reactor by investigating two reaction systems. They reported higher productivity (in gm/min) in micro-reactor vis-à-vis glass tubular reactor and static mixer
Al-Rawashdeh et al. (2012)	8	Barrier-based micro/milli-reactor (BMMR). Gas and liquid are injected into a manifold which distributes each of 8 micro-channels etched on a glass chip	The authors reported a non-uniformity of less than 10%. They reported an optimal operating range of capillary number (Ca) where Taylor (gas–liquid) flow is prevalent. Production capacities of the order of kg/hr can be attained
Dong et al. (2021)	Up to 1000 channels (Miprowa reactor)	External numbering-up Internal numbering-up Sizing up (by increasing length, using geometric similarity or using constant pressure drop)	The authors reviewed various developments and approaches used in scaling up of micro/milli-reactors. They compared the advantages and disadvantages of various scale-up techniques. They disclosed scale-up strategies of Corning Advanced flow reactor technology (1000–10000 tons per annum of API production) and Miprowa reactor (throughout of 300–10000 L/h)
Darekar et al. (2018)	20	External numbering-up. Two incoming reactants streams are split into 20 sub-streams each and each set of sub-streams, a T-shaped microfluidic junction. All these were implemented in a monoblock header (MDIMJ)	The authors achieved a processing throughput of 10 LPH using 20 parallel micro-capillaries (800 micron). They reported a mass transfer coefficient of 4.01 1/s for fine dispersed flow and 0.38 1/s for slug flow regime

of corresponding increase in 1-methylimidazole flow (volumetric) rate. Space–time yield, however, closely follows the trend for product yield. A space–time yield of 1258.4 g/min-L can be obtained using a 300 μm micro-capillary at a reaction temperature of 80 ^{0}C. These experimental trends are substantiated by carrying out numerical simulations involving coupled solution of energy, momentum, and multiple species transport equation in a 2D computational domain. The simulations are able to capture the general experimental trend of effect of temperature, velocity, and tube diameter on product yield. Numerical simulations of micro-channels having obstacles in their flow path are also carried out. The results from these simulations show that microfluidic mixing is indeed important and the designs which promote mixing between the reactants are expected to give better performance for homogeneous reactions. Different designs (reported in literature) of obstacles are studied and the performance of the diamond-shaped obstacles is found to be the best. Finally, possibilities of scale-up of the above-mentioned micro-capillary-based method to meet pilot/commercial-scale production of specialty chemicals like ionic liquids are also discussed.

Supplementary Information The online version contains supplementary material available at https://doi.org/10.1007/s10404-023-02686-9.

Author contributions Nirvik Sen was intrumental in carrying out experiments in microbore tube and setting up CFD models. Dr. K.K. Singh was intrumental in providing valuable inputs for CFD modelling. He wrote the first draft of the paper Dr S. Mukhopadhyay reviewed the manuscript and wrote the final draft of the manuscirpt. K.T Shenoy reviewed the mansucript. He also provided valuable assistance to the first author to carry out experiments in microchannels.

Funding The authors have not received any kind of funding for the research presented.

Data availability The data used and reported in this work can be made available on reasonable request.

Declarations

Conflict of interest The authors confirm that there is no conflict of interest/competing interest in the research work presented for consideration.

References

Alam A, Kim KY (2012) Analysis of mixing in a curved microchannel with rectangular grooves. Chem Eng J 181:708–716

Ali E, Hadj-Kali MK, Alnashef I (2017) Modeling of CO2 solubility in selected imidazolium-based ionic liquids. Chem Eng Commun 204(2):205–215

Al-Rawashdeh M, Yu F, Nijhuis TA, Rebrov EV, Hessel V, Schouten JC (2012) Numbered-up gas–liquid micro/milli channels reactor with modular flow distributor. Chem Eng J 207:645–655

Angeli P, Gobby D, Gavriilidis A (2000) Modelling of gas-liquid catalytic reactions in microchannels. In Microreaction Technology: Industrial Prospects: IMRET 3: Proceedings of the Third International Conference on Microreaction Technology (pp. 253–259). Springer Berlin Heidelberg.

Armand M, Endres F, MacFarlane DR, Ohno H, Scrosati B (2009) Ionic-liquid materials for the electrochemical challenges of the future. Nat Mater 8(8):621–629

Barozzi GS, Pagliarini G (1985) A method to solve conjugate heat transfer problems: the case of fully developed laminar flow in a pipe.

Berg SP, Rovey JL (2013) Decomposition of monopropellant blends of hydroxylammonium nitrate and imidazole-based ionic liquid fuels. J Propuls Power 29(1):125–135

Bhagat AAS, Peterson ET, Papautsky I (2007) A passive planar micromixer with obstructions for mixing at low Reynolds numbers. J Micromech Microeng 17(5):1017

Böwing AG, Jess A (2007) Kinetics and reactor design aspects of the synthesis of ionic liquids—Experimental and theoretical studies for ethylmethylimidazole ethylsulfate. Chem Eng Sci 62(6):1760–1769

Capretto L, Cheng W, Hill M, Zhang X (2011) Micromixing within microfluidic devices. Microfluidics: technologies and applications, pp.27–68

Dai S, Ju YH, Barnes CE (1999) Solvent extraction of strontium nitrate by a crown ether using room-temperature ionic liquids. J Chem Soc, Dalton Trans 8:1201–1202

Darekar M, Singh KK, Sapkale P, Goswami AK, Mukhopadhyay S, Shenoy KT (2018) On microfluidic solvent extraction of uranium. Chem Eng Process: Process Intensif 132:65–74

Dong Z, Wen Z, Zhao F, Kuhn S, Noël T (2021) Scale-up of micro-and milli-reactors: An overview of strategies, design principles and applications. Chem Eng Sci: X 10:100097

Earle MJ, Seddon KR (2000) Ionic liquids. Green solvents for the future. Pure Appl Chem 72(7):1391–1398

Engler M, Kockmann N, Kiefer T, Woias P (2004) Numerical and experimental investigations on liquid mixing in static micromixers. Chem Eng J 101(1–3):315–322

Eβer J, Wasserscheid P, Jess A (2004) Deep Desulphurization on oil refinery streams by extraction with ionic liquids. Green Chem 6:316–322

Fang Y, Ye Y, Shen R, Zhu P, Guo R, Hu Y, Wu L (2012) Mixing enhancement by simple periodic geometric features in microchannels. Chem Eng J 187:306–310

Garg DK, Serra CA, Hoarau Y, Parida D, Bouquey M, Muller R (2015) New transformation proposed for improving CFD simulation of free radical polymerization reactions in microreactors. Microfluid Nanofluid 18:1287–1297

Giridhar P, Venkatesan KA, Subramaniam S, Srinivasan TG, Rao PV (2008) Extraction of uranium (VI) by 1.1 M tri-n-butylphosphate/ionic liquid and the feasibility of recovery by direct electrodeposition from organic phase. J Alloys Compound 448(1–2):104–108

Goswami N, Singh KK, Kar S, Bindal RC, Tewari PK (2014) Numerical simulations of HI decomposition in packed bed membrane reactors. Int J Hydrogen Energy 39(32):18182–18193

Hadj-Kali MK, Althuluth M, Mokraoui S, Wazeer I, Ali E, Richon D (2020) Screening of ionic liquids for gas separation using COSMO-RS and comparison between performances of ionic liquids and aqueous alkanolamine solutions. Chem Eng Commun 207(9):1264–1277

Hessel V, Lob P, Lowe H (2005a) Development of microstructured reactors to enable organic synthesis rather than subduing chemistry. Curr Org Chem 9(8):765–787

Hessel V, Löwe H, Schönfeld F (2005b) Micromixers—a review on passive and active mixing principles. Chem Eng Sci 60(8–9):2479–2501

Jankowski P, Kutaszewicz R, Ogończyk D, Garstecki P (2020) A microfluidic platform for screening and optimization of organic reactions in droplets. Journal of Flow Chemistry 10:397–408

Jayakumar M, Venkatesan KA, Sudha R, Srinivasan TG, Rao PV (2011) Electrodeposition of ruthenium, rhodium and palladium from nitric acid and ionic liquid media: Recovery and surface morphology of the deposits. Mater Chem Phys 128(1–2):141–150

Jess A, GroßeBöwing A, Wasserscheid P (2005) Kinetik und reaktionstechnik der synthese ionischer flüssigkeiten. Chem Ing Tec 77(9):1430–1439

Kang X, Luo C, Wei Q, Xiong C, Chen Q, Chen Y, Ouyang Q (2013) Mass production of highly monodisperse polymeric nanoparticles by parallel flow focusing system. Microfluid Nanofluid 15:337–345

Kar S, Bindal RC, Prabhakar S, Tewari PK (2012) The application of membrane reactor technology in hydrogen production using S-I thermochemical process: a roadmap. Int J Hydrogen Energy 37:3612–3620

Kashid MN, Gupta A, Renken A, Kiwi-Minsker L (2010) Numbering-up and mass transfer studies of liquid–liquid two-phase microstructured reactors. Chem Eng J 158(2):233–240

Kockmann N, Gottsponer M, Roberge DM (2011) Scale-up concept of single-channel microreactors from process development to industrial production. Chem Eng J 167(2–3):718–726

Kulkarni PS, Afonso CA (2010) Deep desulfurization of diesel fuel using ionic liquids: current status and future challenges. Green Chem 12(7):1139–1149

Le Rouzo G, Lamouroux C, Dauvois V, Dannoux A, Legand S, Durand D, Moisy P, Moutiers G (2009) Anion effect on radiochemical stability of room-temperature ionic liquids under gamma irradiation. Dalton Trans 31:6175–6184

Li S, Yan H, Wang Z, Tang Y, Yao Z, Li S (2021) Catalytic Decomposition and Burning of a Dual-Mode Ionic Liquid Propellant. Energy Fuels 35(22):18716–18725

Löb P, Hessel V, Krtschil U (2006) Continuous micro-reactor rigs with capillary sections in organic synthesis: generic process flow sheets, practical experience, and'novel chemistry'. Chim Oggi 24(2):46–50

MacInnes JM (2002) Computation of reacting electrokinetic flow in microchannel geometries. Chem Eng Sci 57(21):4539–4558

Mandal MM, Serra C, Hoarau Y, Nigam KDP (2011) Numerical modeling of polystyrene synthesis in coiled flow inverter. Microfluid Nanofluid 10:415–423

Marsh KN, Boxall JA, Lichtenthaler R (2004) Room temperature ionic liquids and their mixtures—a review. Fluid Phase Equilib 219(1):93–98

Meindersma GW, Podt A, Klaren MB, De Haan AB (2006) Separation of aromatic and aliphatic hydrocarbons with ionic liquids. Chem Eng Commun 193(11):1384–1396

Mou J, Ren Y, Wang J, Wang C, Zou Y, Lou K, Zheng Z, Zhang D (2022) Nickel oxide nanoparticle synthesis and photocatalytic applications: evolution from conventional methods to novel microfluidic approaches. Microfluid Nanofluid 26(4):25

Renken A, Hessel V, Löb P, Miszczuk R, Uerdingen M, Kiwi-Minsker L (2007) Ionic liquid synthesis in a microstructured reactor for process intensification. Chem Eng Process 46(9):840–845

Rout A, Venkatesan KA, Srinivasan TG, Vasudeva Rao PR (2012) Separation of plutonium (IV) from uranium (VI) using phosphonate-based task-specific ionic liquid. Desalin Water Treat 38(1–3):179–183

Sarkar S, Singh KK, Shankar V, Shenoy KT (2014) Numerical simulation of mixing at 1–1 and 1–2 microfluidic junctions. Chem Eng Process 85:227–240

Sen N, Saswani K, Singh KK, Barkade S, Mukhopadhyay S, Chavan SM, Ali SM, Shenoy KT (2017) Extraction of uranium (VI) by tri iso-amyl phosphate (TiAP) in ionic liquids. J Radioanal Nucl Chem 312:255–262

Sen N, Singh KK, Mukhopadhyay S, Shenoy KT, Ghosh SK (2013) Continuous, solvent free, high temperature synthesis of ionic liquid 1-butyl-3-methylimidazolium bromide in a microreactor. BARC Newsletter 334:20–23

Sen N, Singh KK, Mukhopadhyay S, Shenoy KT (2016) Comparison of different microreactors for solvent-free, continuous synthesis of [EMIM][EtSO4] ionic liquid: An experimental and CFD study. J Mol Liq 222:622–631

Sen N, Singh KK, Mukhopadhyay S, Shenoy KT (2022) Microfluidic extraction of uranium from dilute streams using TiAP in ionic liquid as the solvent. Chem Eng Res Des 177:83–95

Serra C, Schlatter G, Sary N, Schönfeld F, Hadziioannou G (2007) Free radical polymerization in multilaminated microreactors: 2D and 3D multiphysics CFD modeling. Microfluid Nanofluid 3:451–461

Shao N, Gavriilidis A, Angeli P (2010) Mass transfer during Taylor flow in microchannels with and without chemical reaction. Chem Eng J 160(3):873–881

Sharma A, Adducci AC, Rovey J, Ma C, Ryan CN, Berg S, Lembeck M, Putnam ZR (2022) Green ionic liquid multimode monopropellant based chemical micro-thruster. In: AIAA SCITECH 2022 Forum (p. 1733).

Shin MS, Park N, Park MJ, Jun KW, Ha KS (2013) Computational fluid dynamics model of a modular multichannel reactor for Fischer-Tropsch synthesis: maximum utilization of catalytic bed by microchannel heat exchangers. Chem Eng J 234:23–32

Uriz I, Arzamendi G, Diéguez PM, Echave FJ, Sanz O, Montes M, Gandía LM (2014) CFD analysis of the effects of the flow distribution and heat losses on the steam reforming of methanol in catalytic (Pd/ZnO) microreactors. Chem Eng J 238:37–44

Wang F, Zhou J, Wang GQ, Zhou XJ (2011) Simulation of methanol steam reforming heated by waste heat for hydrogen production in a microreactor. In: Advanced materials research (Vol. 216, pp. 718–722). Trans Tech Publications Ltd.

Waterkamp DA, Heiland M, Schlüter M, Sauvageau JC, Beyersdorff T, Thöming J (2007) Synthesis of ionic liquids in micro-reactors—a process intensification study. Green Chem 9(10):1084–1090

Waterkamp DA, Engelbert M, Thoeming J (2009) On the effect of enhanced mass transfer on side reactions in capillary microreactors during high-temperature synthesis of an ionic liquid. Chem Eng Technol: Indus Chem-Plant Equip-Process Eng-Biotechnol 32(11):1717–1723

Whitmore S, Merkley D, Eilers S, Taylor T (2013) Hydrocarbon-Seeded Ignition System for Small Spacecraft Thrusters Using Ionic Liquid Propellants.

Willmes S, Jess A (2013) Efficient continuous production of ionic liquids in a loop reactor–Experimental and theoretical studies for the example of 1-ethyl-3-methylimidazolium ethyl sulphate. Chem Eng J 222:198–208

Xu D, Zhang M, Gao J, Zhang L, Zhou S, Wang Y (2019) Separation of heterocyclic nitrogen compounds from coal tar fractions via ionic liquids: COSMO-SAC screening and experimental study. Chem Eng Commun 206(9):1199–1217

Ye Z, Jia X, Lou M, Huang H, Lu P, Ye G, Gong X, Zhu Y, Yan B (2022) Surface-enhanced Raman scattering substrates prepared by controlled synthesis of gold nanobipyramids in microchannels. Microfluid Nanofluid 26(4):28

Zhang S, Sun N, He X, Lu X, Zhang X (2006) Physical properties of ionic liquids: database and evaluation. J Phys Chem Ref Data 35(4):1475–1517

Zhang Y, Jiang W, Wang L (2010) Microfluidic synthesis of copper nanofluids. Microfluid Nanofluid 9:727–735

Zhao H (2006) Innovative applications of ionic liquids as "green" engineering liquids. Chem Eng Commun 193(12):1660–1677